Nonlinear Dyn (2014) 78:1765–1779
DOI 10.1007/s11071-014-1553-4

ORIGINAL PAPER

An extended traffic flow model on a gradient highway with the consideration of the relative velocity

Jie Zhou · Zhong-Ke Shi · Jin-Liang Cao

Received: 12 October 2013 / Accepted: 18 June 2014 / Published online: 11 July 2014

Abstract In this paper, an extended traffic flow model on a single-lane gradient highway is proposed with the consideration of the relative velocity. The stability condition is obtained by the use of linear stability analysis. It is shown that the stability of traffic flow on the gradient varies with the slope and the coefficient of the relative velocity: when the slope is constant, the stable regions increase with the increase of the coefficient of the relative velocity; when the coefficient of the relative velocity is constant, the stable regions increase with the decrease of the slope in downhill and increase with the increase of the slope in uphill. The Burgers, Korteweg-de Vries, and modified Korteweg-de Vries equations are derived to describe the triangular shock waves, soliton waves, and kink-antikink waves in the stable, metastable, and unstable region, respectively. The numerical simulation shows a good agreement with the analytical result, which shows that the traffic congestion can be suppressed by introducing the relative velocity.

Keywords Slope · Relative velocity · Nonlinear analysis · Gradient highway · Density wave

J. Zhou (✉) · Z.-K. Shi · J.-L. Cao
College of Automation, Northwestern Polytechnical University, Xi'an 210097, Shanxi, China
e-mail: zhoujie@zjou.edu.cn

1 Introduction

Traffic problems have attracted considerable attentions especially traffic jams in recent decades. To investigate the properties of traffic jams, various traffic flow models including car-following models, cellular automation models, hydrodynamics models, and gas kinetics models were proposed by many scholars with different backgrounds [1–34].

The car-following models explain many complex physical phenomena in traffic flow. Bando et al. [2] proposed an optimal velocity model (OVM) to describe the dynamical behaviors of vehicles on a highway under a high-density condition. But the comparison with field data showed that high acceleration and unrealistic deceleration appear in OVM. To overcome this shortage, Helbing and Tilch [3] developed a generalized force model (GFM) with a velocity difference term added into the OVM. Jiang et al. [4,5] proposed a full velocity difference model (FVDM) which considers more aspects in the car-following process than the OVM and the GFM. Xue et al. [6] extended the OVM to take the effects of the relative velocity into account. Recently, Peng et al. [7] proposed an optimal velocity difference model (OVDM) to study the effect of the optimal velocity difference.

The nonlinear waves in traffic flow have been investigated by using nonlinear analysis. Kerner et al. [8] had found the single pulse density waves in the numerical simulation with the hydrodynamic model. Kurtze and Hong [9] had shown that the single pulse den-

sity wave is a soliton. Komatsu and Sasa [10] derived modified Korteweg-de Vries (MKdV) equation from OVM to describe the traffic jams in terms of the kink density waves. Nagatani [11] improved OVM by taking the effect of the next-nearest-neighbor interaction into account and found that triangular shockwave, soliton wave, and kink-antikink wave appear. Xue [13] extended OVM based on Jiang's full velocity difference model and discussed its stability and density waves analytically and numerically. Ge et al. [14] proposed an extended model by incorporating intelligent transportation applications and analyzed it by using linear stability theory and nonlinear analysis. The kink-antikink solutions were obtained near the critical point in the unstable region.

All the above works are based on the highway with no slope. But in real traffic, the road may not be flat. Li et al. [17] investigated the effect of the slope in a single-lane highway on the traffic flow with an extended optimal velocity model. Komada et al. [18] considered the effect of gravitational force upon traffic flow on a highway with sags, uphill, and downhill. The gravitational force was considered as an external force acting on vehicles. They investigated the traffic states and jamming transitions induced by the slope of the highway and derived the fundamental diagram for the traffic flow on the sag. Zhu et al. [20] investigated the stability and density waves of the traffic flow on a gradient highway with different slopes. But these work did not consider the effect of the relative velocity. In real traffic, the vehicle will not brake if the preceding cars are faster, even if the headway is smaller than the safe distance.

The paper is organized as follows. In Sect. 2, the model is formulated, and the stability analysis is obtained. We can see the stability condition varies with the slope and the coefficient of the relative velocity. In Sect. 3, the Burgers, KdV, and MKdV equations are derived in three types of traffic flow regions by using nonlinear analysis. The numerical simulations are given in Sect. 4.

2 Model and linear stability

We consider a situation such that many same vehicles move ahead on a single-lane highway. A gradient is positioned on the single-lane highway. Traffic flow is under a periodic boundary condition. The gravitational force acts upon vehicles on the slope of the gradient. Figure 1 shows the illustration of gravitational force acting upon a vehicle on an uphill and downhill highway, respectively [20]. The slope of the gradient is represented by θ, the gravity is g, and the mass of a vehicle is m. Then, the external force $mg\sin\theta$ acts on the vehicle in a horizontal direction when a driver does not operate the brake. If a driver operates the brake, the gravitational force is reduced by the brake control.

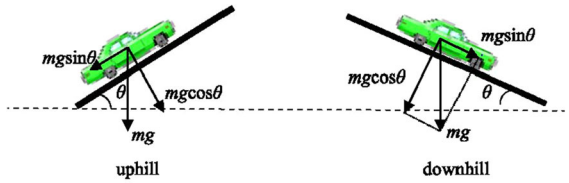

Fig. 1 Illustration of the gravitational force acting upon a vehicle on a gradient: uphill and downhill

The equation of motion for vehicle n is described by

$$m\frac{\mathrm{d}^2x_n(t)}{\mathrm{d}t^2} = F(\Delta x_n(t), \Delta v_n(t)) - \mu\frac{\mathrm{d}x_n(t)}{\mathrm{d}t} - mg\sin\theta B(\Delta x_n(t)), \tag{1}$$

where $x_n(t)$ is the position of vehicle n at time t, $\Delta x_n(t) = x_{n+1}(t) - x_n(t)$ and $\Delta v_n(t) = v_{n+1}(t) - v_n(t)$ are the headway and the velocity difference between preceding vehicle $n+1$ and the following vehicle n, respectively, $F(\Delta x_n(t), \Delta v_n(t))$ is the driving force, μ is the friction coefficient, and $B(\Delta x_n(t))$ is the brake-control function. Here, we assume that the driving force is the function of the headway $\Delta x_n(t)$ and the relative velocity $\Delta v_n(t)$, because the driving force is given by drivers, and drivers adjust the driving force by considering not only the headway but also the relative velocity. The brake-control function $B(\Delta x_n(t))$ is the function of the headway $\Delta x_n(t)$, it represents the effect when a driver operates the brake when the headway varies [18], when $\Delta x_n(t) \to 0$, the vehicle should stop to avoid collision, we assume $B(\Delta x_n(t)) \to 0$ for $\Delta x_n(t) \to 0$. When the headway is sufficient large ($\Delta x_n(t) \to \infty$), the vehicle will never brake, and the gravitational force acting on the vehicle is $mg\sin\theta$, that means $B(\Delta x_n(t)) \to 1$ for $\Delta x_n(t) \to \infty$. Here we consider $F(\Delta x_n(t), \Delta v_n(t))$ is the linear function of $\Delta x_n(t)$ and $\Delta v_n(t)$, that is

$$F(\Delta x_n(t), \Delta v_n(t)) = \alpha F(\Delta x_n(t)) + \beta F(\Delta v_n(t)).$$

Then, Eq. (1) is rewritten as

$$\frac{\mathrm{d}^2x_n(t)}{\mathrm{d}t^2} = \frac{\mu}{m}\left[\frac{\alpha F(\Delta x_n(t))}{\mu} - \frac{mg\sin\theta B(\Delta x_n(t))}{\mu} - \frac{\mathrm{d}x_n(t)}{\mathrm{d}t}\right] + \frac{\beta}{m}F(\Delta v_n(t)), \tag{2}$$

we compare Eq. (2) with the conventional FVDM. It is described by [4]

$$\frac{\mathrm{d}^2x_n(t)}{\mathrm{d}t^2} = a\left[V(\Delta x_n(t)) - \frac{\mathrm{d}x_n(t)}{\mathrm{d}t}\right] + \lambda a\Delta v_n(t). \tag{3}$$

with

$$V(\Delta x_n(t)) = \frac{v_{f,\max}}{2}[\tanh(\Delta x_n(t) - h_c) + \tanh(h_c)], \tag{4}$$

where $v_{f,\max}$ is the maximal velocity without any slope. When $\theta = 0$ in Eq. (2), it should reduce to Eq. (3). Therefore, we set

$$\frac{\mu}{m} = a, \qquad \lambda = \frac{\beta}{\mu}, \tag{5}$$

$$\frac{\alpha F(\Delta x_n(t))}{\mu} = \frac{v_{f,\max}}{2}[\tanh(\Delta x_n(t) - h_c) + \tanh(h_c)], \tag{6}$$

$$\frac{\beta}{m}F(\Delta v_n(t)) = \lambda a\Delta v_n(t). \tag{7}$$

In Ref. [18], the term $\frac{mg\sin\theta B(\Delta x_n(t))}{\mu}$ in Eq. (2) is given by

$$\frac{mg\sin\theta B(\Delta x_n)}{\mu} = V_g(\Delta x_n) = \frac{v_{g,\max}}{2}[\tanh(\Delta x_n - h_b) + \tanh(h_b)] \tag{8}$$

where $v_{g,\max} = \frac{mg\sin\theta}{\mu}$. The turning point h_b is the brake distance. $v_{g,\max}$ is proportional to slope $\sin\theta$. Thus, the effect of the slope is taken into account in $v_{g,\max}$ of Eq. (8). And the extended optimal velocity $V(\Delta x_n)$ is given by [18]

$$V(\Delta x_n) = \frac{v_{f,\max}}{2}[\tanh(\Delta x_n - h_c) + \tanh(h_c)], \tag{9}$$

for a highway without slope,

$$V(\Delta x_n) = \frac{v_{f,\max}}{2}[\tanh(\Delta x_n - h_c) + \tanh(h_c)] - \frac{v_{g,u,\max}}{2}[\tanh(\Delta x_n - h_{b,u}) + \tanh(h_{b,u})], \tag{10}$$

for an uphill gradient highway, and

$$V(\Delta x_n) = \frac{v_{f,\max}}{2}[\tanh(\Delta x_n - h_c) + \tanh(h_c)] + \frac{v_{g,d,\max}}{2}[\tanh(\Delta x_n - h_{b,d}) + \tanh(h_{b,d})], \tag{11}$$

for a downhill gradient highway. But the term h_c in Eqs. (10) and (11) is not taken the slope effect into account, and we think h_c should be influence by the slope. So we let the h_c be rewritten as $h_{c,\theta}$, and $h_{c,\theta} = h_c(1-\xi\sin\theta)$ for uphill and $h_{c,\theta} = h_c(1+\eta\sin\theta)$ for downhill [20], when $\theta = 0$, $h_{c,\theta}$ reduce to h_c. For simplicity, here we set $\xi = \eta = 1$. $v_{g,u,\max}$ and $v_{g,d,\max}$ are the maximal reduced and enhanced velocity on uphill and downhill gradients which are formulated as $v_{g,u,\max} = v_{g,d,\max} = v_{g,\max}$, when $\theta = 0$, $v_{g,\max} = 0$.

Thus, the extended full velocity difference model is obtained

$$\frac{\mathrm{d}^2x_n(t)}{\mathrm{d}t^2} = a\left[V(\Delta x_n(t)) - \frac{\mathrm{d}x_n(t)}{\mathrm{d}t}\right] + \lambda a\Delta v_n(t), \tag{12}$$

with the extended optimal velocity

$$V(\Delta x_n) = \frac{v_{f,\max} \mp v_{g,\max}}{2}[\tanh(\Delta x_n - h_{c,\theta}) + \tanh(h_{c,\theta})]. \tag{13}$$

The sign $'-'$ represents uphill, and the sign $'+'$ represents downhill. $h_{c,\theta} = h_c(1 \mp \sin\theta)$ is the safety distance, the sign $'-'$ also represents uphill, and the sign $'+'$ represents downhill. When $\theta = 0$, the extended FVDM and optimal velocity are the conventional FVDM and optimal velocity.

Now we deduce the stability condition of the extended FVDM. Here we select $v_{f,\max} = 4$, $\frac{mg}{\mu} = 1$, $v_{g,\max} = \sin\theta$. In order to investigate the stability of the traffic flow on an uphill/downhill highway we assume that N vehicles move homogeneously on a circular lane with length L and slope θ. The slope θ is

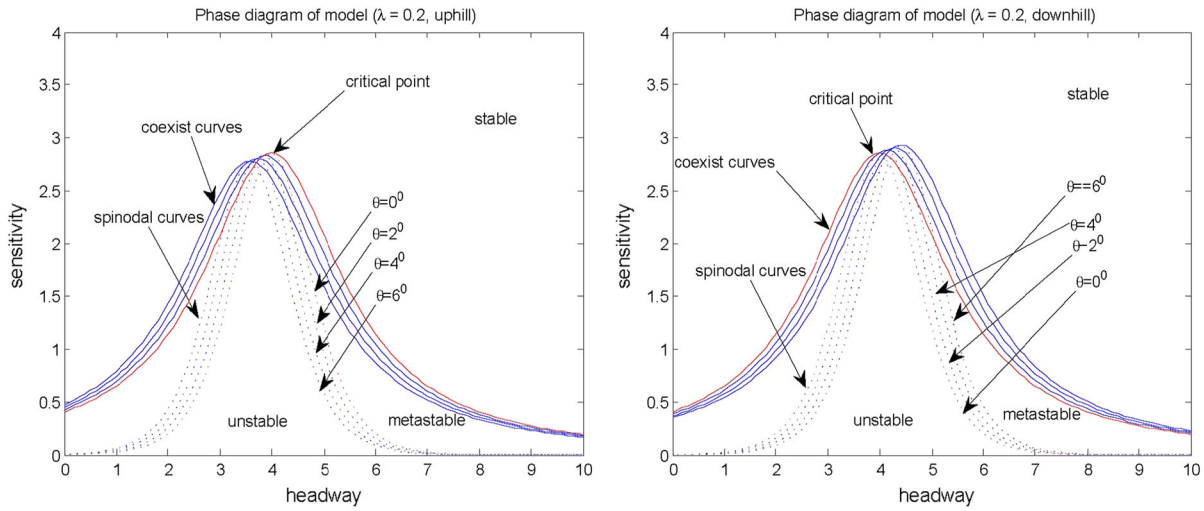

Fig. 2 Illustration of the phase diagram of the model with different θ on a gradient uphill and downhill

between 0° and 6° according to the real highway situation. Assume

$$V_0(\Delta x_n) = \tanh(\Delta x_n - h_{c,\theta}) + \tanh(h_{c,\theta}). \tag{14}$$

The Eq. (13) has the following formation

$$V(\Delta x_n) = \frac{4 \mp \sin\theta}{2} V_0(\Delta x_n). \tag{15}$$

Then Eq. (12) can be rewritten as

$$\frac{\mathrm{d}^2 x_n}{\mathrm{d}t^2} = a\left[\frac{4 \mp \sin\theta}{2} V_0(\Delta x_n) - \frac{\mathrm{d}x_n}{\mathrm{d}t}\right] + \lambda a \Delta v_n. \tag{16}$$

We apply the linear stability theory to analyze the traffic model described by Eq. (16). Supposing the vehicles running with the uniform headway h and optimal velocity $V(h)$, then we get the uniform steady state solution $x_n^{(0)}(t)$ for Eq. (16)

$$x_n^{(0)}(t) = hn + \frac{4 \mp \sin\theta}{2} V_0(h)t. \tag{17}$$

Assuming $x_n(t)$ be a small deviation from the uniform steady state $x_n^{(0)}(t) : x_n(t) = x_n^{(0)}(t) + y_n(t)$ where $y_n(t)$ is the small deviation. Inserting it and Eq. (17) into Eq. (16), then the linearized equation for $y_n(t)$ is obtained from Eq. (16)

$$\frac{\mathrm{d}^2 y_n}{\mathrm{d}t^2} = a\left[\frac{4 \mp \sin\theta}{2} V_0'(h)\Delta y_n - \frac{\mathrm{d}y_n}{\mathrm{d}t}\right] + \lambda a \frac{\mathrm{d}\Delta y_n}{\mathrm{d}t} \tag{18}$$

where $\Delta y_n = y_{n+1}(t) - y_n(t)$, and $V_0'(h)$ is the derivative of optimal velocity function $V_0(h)$ at point $\Delta x_n(t) = h$.

The stability condition is obtained by the same method in Ref. [6]

$$V_0'(h) < a\frac{1 + 2\lambda}{4 \mp \sin\theta}. \tag{19}$$

Then the neutral stability condition is given by

$$a_s = \frac{4 \mp \sin\theta}{1 + 2\lambda} V_0'(h). \tag{20}$$

The spinodal stability curves for different slopes of the gradient highway are shown in Fig. 2. Here we select $\lambda = 0.2$. From Fig. 2 we can see that the dotted lines are the spinodal stability curves, and the solid lines are coexisting curves. The areas below the spinodal stability curves are unstable regions, and the areas above the coexisting curves are stable regions. The areas between the spinodal stability curves and coexisting curves are metastable regions. Figure 2 shows the spinodal stability curves and coexisting curves for uphill and downhill on highways, respectively. In the downhill situations the stable region increases with the decrease of the slope, while in the uphill situations the stable

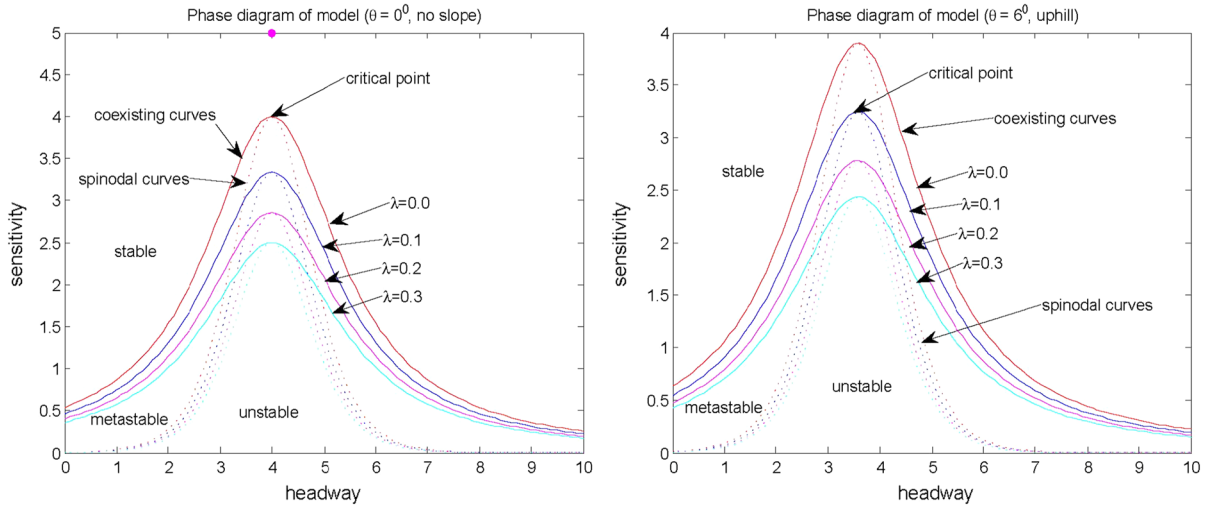

Fig. 3 Illustration of the phase diagram of the model with different λ on a gradient uphill

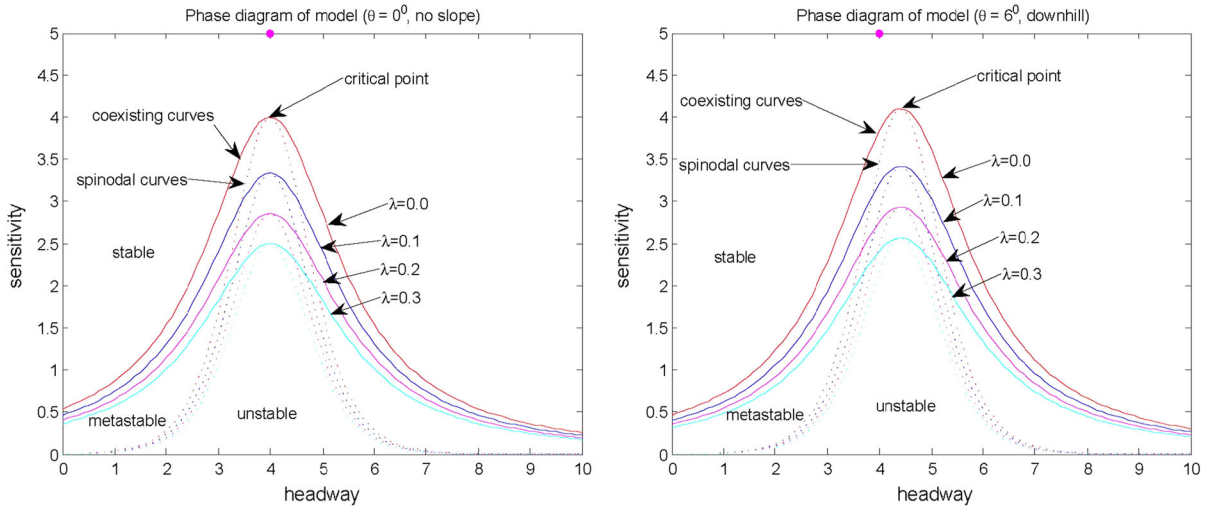

Fig. 4 Illustration of the phase diagram of the model with different λ on a gradient downhill

region increases with the increase of the slope. So the stability of the traffic flow varies with the slopes of the gradient. In addition one can see that the apexes of the spinodal stability curves are the critical points (h_c, a_c) which are corresponding to different slope θ. Obviously safety distances $h_c = 4, 3.86, 3.72, 3.58$ in uphill situations and $h_c = 4, 4.14, 4.28, 4.42$ in downhill situations are corresponding to slopes $\theta = 0°, 2°, 4°, 6°$, respectively. The results agree with ones in Ref. [20].

Figures 3 and 4 show the phase diagram with different values of λ on uphill and downhill situation, respectively. Here we select $\theta = 0°, 6°$. From Figs. 3 and 4, we can see that the critical points rise with decreasing λ. The traffic flow is more stable with the increase of λ. In Sect. 4, we perform numerical simulations to study the impact of small perturbations to the whole traffic flow with different λ.

3 Nonlinear analysis

In this section, by using the reductive perturbation method introduced in Ref. [10], we derive the Burgers, KdV, and MKdV equations in the stable, metastable,

and unstable regions, respectively. For later convenience, Eq. (16) can be rewritten as

$$\begin{aligned}\frac{\mathrm{d}^2\Delta x_n(t)}{\mathrm{d}t^2} &= a\left\{\left[\frac{4\mp\sin\theta}{2}V_0(\Delta x_{n+1}(t)) - V_0(\Delta x_n(t))\right]\right. \\ &\quad \left. - \frac{\mathrm{d}\Delta x_n(t)}{\mathrm{d}t}\right\} + a\lambda\left[\frac{\mathrm{d}\Delta x_{n+1}(t)}{\mathrm{d}t} - \frac{\mathrm{d}\Delta x_n(t)}{\mathrm{d}t}\right].\end{aligned} \tag{21}$$

We introduce slow scales for space variable n and time variable t and define low variables X and T for $0 < \varepsilon \ll 1$ [21]

$$X = \varepsilon(n + bt), \qquad T = \varepsilon^m t \tag{22}$$

where b is a constant to be determined. Assuming

$$\Delta x_n(t) = h + \varepsilon^l R(X, T). \tag{23}$$

The values of the index m, l represent different phases of the traffic flow. Three groups of values $m = 2, l = 1$; $m = 3, l = 2$; $m = 3, l = 1$ are corresponding to the stable traffic flow region, metastable traffic flow region, and unstable traffic flow region, respectively.

By Substituting Eqs. (22)-(23) into Eq. (21) and expanding to the $m + l + 1$ order of ε, we obtain the following nonlinear partial differential equation:

$$\begin{aligned}&a\varepsilon^{l+1}\Big(b - kV_0'(h)\Big)\partial_X R \\ &+\varepsilon^{l+2}\Big(b^2 - \frac{ak}{2}V_0'(h) - ab\lambda\Big)\partial_X^2 R \\ &+\varepsilon^{l+3}\Big(-\frac{ak}{6}V_0'(h) - \frac{ab\lambda}{2}\Big)\partial_X^3 R \\ &+\varepsilon^{l+4}\Big(-\frac{ak}{24}V_0'(h) - \frac{ab\lambda}{6}\Big)\partial_X^4 R \\ &+\varepsilon^{2l+1}\Big(-\frac{ak}{2}V_0''(h)\Big)\partial_X R^2 \\ &+\varepsilon^{2l+2}\Big(-\frac{ak}{4}V_0''(h)\Big)\partial_X^2 R^2 \\ &+\varepsilon^{3l+1}\Big(-\frac{ak}{6}V_0'''(h)\Big)\partial_X R^3 \\ &+\varepsilon^{3l+2}\Big(-\frac{ak}{12}V_0'''(h)\Big)\partial_X^2 R^3 \\ &+\varepsilon^{m+l}a\partial_T R + \varepsilon^{m+l+1}(2b - \lambda a)\partial_X\partial_T R = 0\end{aligned} \tag{24}$$

where $k = \frac{4\mp\sin\theta}{2}$.

First, we discuss the triangular shock waves of the traffic flow in the stable region. The nonlinear partial differential equation is obtained from Eq. (24) for $m = 2, l = 1$.

$$\begin{aligned}&\varepsilon^2 a\Big(b - kV_0'(h)\Big)\partial_X R + \varepsilon^3\Big[a\partial_T R - \frac{ak}{2}V_0''(h)\partial_X R^2 \\ &+\Big(b^2 - \frac{ak}{2}V_0'(h) - ab\lambda\Big)\partial_X^2 R\Big] = 0\end{aligned} \tag{25}$$

Taking $b = kV_0'(h)$, the second-order terms of ε is eliminated in Eq. (25). We obtain the following partial differential equation:

$$\begin{aligned}&\partial_T R - kV_0''(h)R\partial_X R \\ &= \left(\frac{1+2\lambda}{2} - \frac{kV_0'(h)}{a}\right)kV_0'(h)\partial_X^2 R\end{aligned} \tag{26}$$

In accordance with criterion Eq. (19), the coefficient of the second derivative of Eq. (26) is positive in the stable region. Therefore, in the stable region, Eq. (26) is just the Burgers equation. If $R(X, 0)$ is of compact support, then the solution $R(X, T)$ of Eq. (26) is

$$\begin{aligned}R(X,T) = &\frac{1}{|kV_0''(h)|T}\left[X - \frac{\eta_{n+1}+\eta_n}{2}\right] \\ &- \frac{\eta_{n+1}-\eta_n}{2|kV_0''(h)|T}\tanh\left[\left(\frac{1+2\lambda}{2}\right.\right. \\ &\left.\left. - \frac{kV_0'(h)}{a}\right)kV_0'(h)\frac{(\eta_{n+1}-\eta_n)(X-\xi_n)}{4|kV_0''(h)|T}\right]\end{aligned} \tag{27}$$

where ξ_n are the coordinates of the shock fronts, and η_n are the coordinates of the intersections of the slopes with the x-axis ($n = 1, 2, ..., N$). As $O(\frac{1}{T})$, $R(X, T)$ decays to 0 when $T \to +\infty$. That means any shock wave expressed by Eq. (27) in stable traffic flow region will evolve to a uniform flow when time is sufficient large. We see this phenomenon when $\lambda = 0.2$ in Figs. 5, 6, and 7 of Sect. 4.

Second, we discuss the soliton waves of the traffic flow in the metastable region. The nonlinear partial differential equation is obtained from Eq. (24) for $m = 3, l = 2$.

$$\begin{aligned}&\varepsilon^3 a\Big(b - kV_0'(h)\Big)\partial_X R \\ &+\varepsilon^4\Big(b^2 - \frac{aV_0'(h)k}{2} - \lambda ab\Big)\partial_X^2 R \\ &+\varepsilon^5 a\left[\partial_T R - \left(\frac{V_0'(h)k}{6} + \frac{\lambda b}{2}\right)\partial_X^3 R\right.\end{aligned}$$

$$-\frac{V_0''(h)k}{2}\partial_X R^2\Big]\varepsilon^6\Big[(2b-a\lambda)\partial_X\partial_T R - \left(\frac{aV_0'(h)k}{24}+\frac{\lambda ab}{6}\right)\partial_X^4 R - \frac{aV_0''(h)k}{4}\partial_X^2 R^2\Big] = 0. \tag{28}$$

Near the neutral stability line in the unstable region, let

$$\frac{a_s}{a} = 1+\varepsilon^2 \tag{29}$$

where a_s is given by Eq. (20). By taking $b = kV_0'(h)$, the third- and fourth-order terms of ε are eliminated from Eq. (28), and Eq. (28) can be rewritten as

$$\begin{aligned}&\varepsilon^5\left[\partial_T R - f_1\partial_X^3 R - f_2 R\partial_X R\right]\\ &+\varepsilon^6\left[-f_3\partial_X^2 R + f_4\partial_X^2 R^2 + f_5\partial_X^4 R\right] = 0\end{aligned} \tag{30}$$

where

$$\begin{aligned}f_1 &= \frac{1+3\lambda}{6}kV_0'(h), \qquad f_2 = kV_0''(h),\\ f_3 &= -\frac{1+2\lambda}{2}kV_0'(h),\\ f_4 &= \left(\frac{kV_0'(h)}{a}-\frac{1+2\lambda}{4}\right)kV_0''(h),\\ f_5 &= kV_0'(h)[2kV_0'(h)-a\lambda]\frac{1+3\lambda}{6a} - kV_0'(h)\frac{1+4\lambda}{24}.\end{aligned}$$

In order to derive the standard KdV equation with higher-order correction, we make the following transformation in Eq. (30)

$$T = \sqrt{f_1}T_k, \qquad X = -\sqrt{f_1}X_k, \qquad R = \frac{1}{f_2}R_k. \tag{31}$$

By using of Eq. (31), we obtain the standard KdV equation with higher-order correction term

$$\partial_{T_k}R_k + \partial_{X_k}^3 R_k + R_k\partial_{X_k}R_k + \frac{\varepsilon}{\sqrt{f_1}}\left[-f_3\partial_{X_k}^2 R_k + \frac{f_4}{f_2}\partial_{X_k}^2 R_k^2 + \frac{f_5}{f_1}\partial_{X_k}^4 R_k\right] = 0. \tag{32}$$

Next, we assume that $R_k(X_k,T_k) = R_0(X_k,T_k) + \varepsilon R_1(X_k,T_k)$ to consider the $O(\varepsilon)$ correction in Eq. (32). If we ignore the $O(\varepsilon)$ term in Eq. (32), it is just the KdV equation with the soliton solution

$$R_0(X_k,T_k) = A\,\mathrm{sech}^2\left[\sqrt{\frac{A}{12}}\left(X_k - \frac{A}{3}T_k\right)\right] \tag{33}$$

where A is a free parameter. It is the amplitude of soliton solutions of the KdV equation. The perturbation term in Eq. (32) gives the condition of selecting a unique member from the continuous family of KdV solitons. In order to obtain the value of A, the solvability condition is

$$(R_0, M[R_0]) \equiv \int_{-\infty}^{\infty} \mathrm{d}X_k R_0 M[R_0] = 0 \tag{34}$$

must be satisfied, here $M[R_0]$ is the $O(\varepsilon)$ term in Eq. (32). By computing the integration in Eq. (34), we obtain the value of amplitude A

$$A = \frac{21 f_1 f_2 f_3}{24 f_1 f_4 - 5 f_2 f_5}. \tag{35}$$

Substituting the values of f_1–f_5 into Eq. (35), we get the value of A. Substituting each variable by the original one, we obtain the soliton solution of the headway

$$\begin{aligned}\Delta x_n(t) = h + \frac{A}{f_2}\left(\frac{a_s}{a}-1\right)&\\ \mathrm{sech}^2\left[\sqrt{\frac{A}{12f_1}\left(\frac{a_s}{a}-1\right)}\,(n + c_1 t\right.&\\ \left.+\frac{A}{3}\left(\frac{a_s}{a}-1\right)t\right)\Big].&\end{aligned} \tag{36}$$

Now, we have derived the soliton density wave described by the KdV equation near the neutral stability line.

Finally, we discuss the kink-antikink waves of the traffic flow in the unstable region. The critical point in Figs. 3 and 4 is the turning point where $V_0''(h_c) = 0$. The nonlinear partial differential equation is obtained from Eq. (24) for $m = 3, l = 1$.

$$\begin{aligned}&\varepsilon^2 a\Big(b - kV_0'(h)\Big)\partial_X R\\ &+\varepsilon^3\Big(b^2 - \frac{akV_0'(h)}{2} - \lambda ab\Big)\partial_X^2 R\\ &+\varepsilon^4 a\left[\partial_T R - \left(\frac{kV_0'(h)}{6}+\frac{\lambda b}{2}\right)\partial_X^3 R\right.\end{aligned}$$

$$-\frac{kV_0'''(h)}{3}\partial_X R^3\Big]$$
$$+\varepsilon^5\Big[(2b-a\lambda)\partial_X\partial_T R-\frac{akV_0'(h)+4\lambda ab}{24}\partial_X^4 R$$
$$-\frac{akV_0'''(h)}{6}\partial_X^2 R^3\Big]=0. \tag{37}$$

Supposing

$$\frac{a_c}{a}=1+\varepsilon^2 \tag{38}$$

for a near the critical point (h_c, a_c), where $a_c=\frac{4\mp\sin\theta}{1+2\lambda}$. Let $b=\frac{4\mp\sin\theta}{2}V_0'(h)$, the second- and third-order terms of ε can be eliminated from Eq. (37). Then Eq. (37) can be rewritten as

$$\varepsilon^4\left[\partial_T R-g_1\partial_X^3 R+g_2\partial_X R^3\right]$$
$$+\varepsilon^5\left[g_3\partial_X^2 R+g_4\partial_X^2 R^3+g_5\partial_X^4 R\right]=0 \tag{39}$$

where

$$g_1=\frac{1+3\lambda}{6}kV_0'(h),\qquad g_2=-\frac{kV_0'''(h)}{6},$$
$$g_3=\frac{1+2\lambda}{2}kV_0'(h),$$
$$g_4=\left(\frac{kV_0'(h)}{3a}-\frac{1+2\lambda}{12}\right)kV_0'''(h),$$
$$g_5=\frac{1+3\lambda}{6a}kV_0'(h)[2kV_0'(h)-a\lambda]-\frac{1+4\lambda}{24}kV_0'(h).$$

In order to derive the standard mKdV equation with higher-order correction, we make the following transformation in Eq. (39)

$$T=\frac{1}{g_1}T_m,\qquad R=\sqrt{\frac{g_1}{g_2}}R_m. \tag{40}$$

Then we obtain the standard MKdV equation with higher-order correction term

$$\partial_{T_m}R_m-\partial_X^3 R_m+\partial_X R_m^3$$
$$+\frac{\varepsilon}{g_1}\left[g_3\partial_X^2 R_m+\frac{g_1g_4}{g_2}\partial_X^2 R_m^3+g_5\partial_X^4 R_m\right]=0. \tag{41}$$

If we ignore the $O(\varepsilon)$ term in Eq. (41), it is just the MKdV equation with the kink-antikink solution

$$R_{m0}(X,T_m)=\sqrt{B}\tanh\sqrt{\frac{B}{2}}(X-BT_m). \tag{42}$$

Similar to the process of deriving the amplitude A for KdV equation, we obtain the value of propagation velocity B for the kink-antikink solution as follows:

$$B=\frac{5g_2g_3}{2g_2g_5-3g_1g_4} \tag{43}$$

which is the same as the one in Ref. [22]. Inserting Eq. (40) into Eq. (42), we get the solution of the MKdV equation

$$R(X,T)=\sqrt{\frac{g_1B}{g_2}}\tanh\sqrt{\frac{B}{2}}(X-Bg_1T). \tag{44}$$

Then we gain the kink-antikink solution of the headway

$$\Delta x_n=h+\sqrt{\frac{g_1B}{g_2}(\frac{a_c}{a}-1)}$$
$$\tanh\left[\sqrt{\frac{B}{2}(\frac{a_c}{a}-1)}(n+c_1t-Bg_1(\frac{a_c}{a}-1)t)\right]. \tag{45}$$

And the amplitude C of the kink-antikink solution equation (45) is given by

$$C=\sqrt{\frac{g_1B}{g_2}\left(\frac{a_c}{a}-1\right)}.$$

The kink solution represents the coexisting phase, which consists of the freely moving phase with low density and the congested phase with high density. The headway of the freely moving phase and the jammed phase is given by $\Delta x=h_c+C$ and $\Delta x=h_c-C$, respectively. Therefore, we get the coexisting curve in the $(\Delta x, a)$ plane (see Figs. 2, 3, 4).

4 Numerical simulations

To check the theoretical results, we carry out numerical simulations for the second-order differential equation (12). The boundary conditions selected are periodic

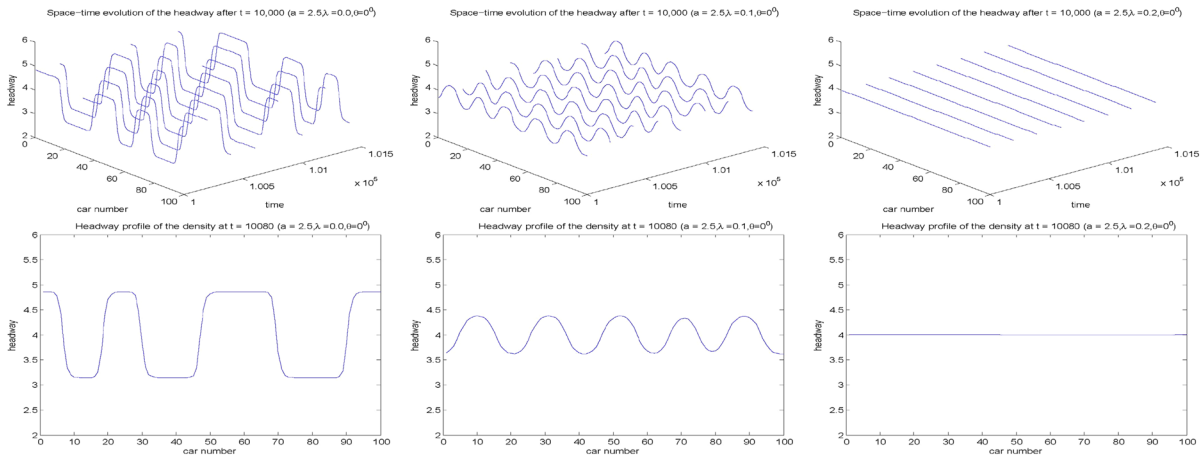

Fig. 5 Space–time evolution after $t = 10,000$ and corresponding headway at $t = 10,080$ of the density wave with no slope

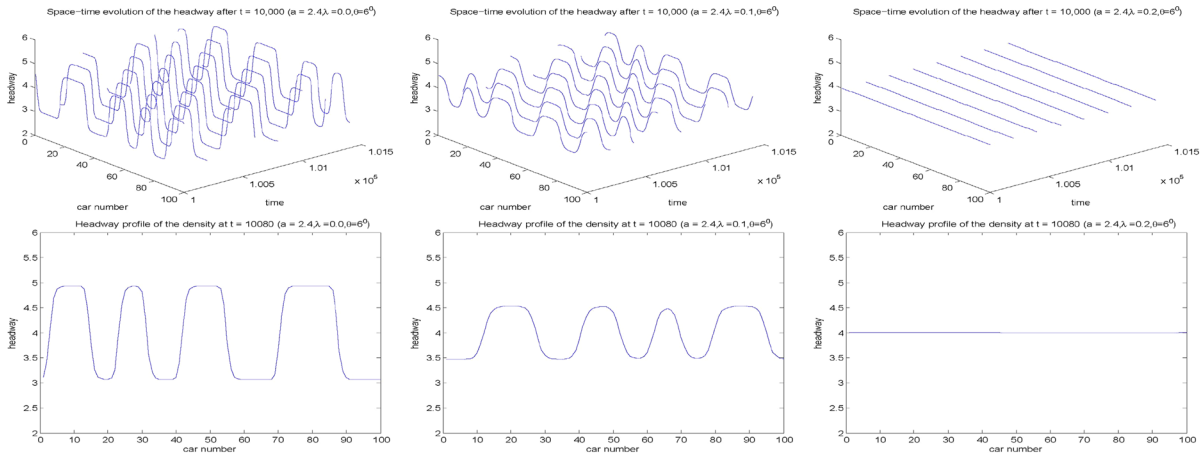

Fig. 6 Space–time evolution after $t = 10,000$ and corresponding headway at $t = 10,080$ of the density wave on a uphill slope 6°

ones. We investigate the impact of local small disturbances to the whole system with different λ. The uniform flow is such that the vehicles move with the constant headway $h = 4.0$, and the initial conditions are

$$x_n(0) = 4.0 (n \neq 50, 51), \quad x_n(0) = 4.0 - 0.1 (n = 50),$$
$$x_n(0) = 4.0 + 0.1 (n = 51)$$

where the total number of cars is $N = 100$, $h_c = 4.0$, $v_{f,\max} = 4.0$, the slope $\theta = 0°$ for no slope, and $\theta = 6°$ for uphill and downhill.

Figure 5 shows the typical traffic patterns after a sufficiently long time $t = 10^4$ with different λ for $a = 2.5$ on no slope highway. Figure 5 exhibits the time evolution of the headway and correspond headway profile obtained at $t = 10,080$ for $\lambda = 0.0, 0.1, 0.2$. By using the linear stability condition (19), the traffic flow is linear unstable for $\lambda = 0.0, 0.1$. The traffic flow is stable for $\lambda = 0.2$. So the small disturbances will be amplified, and the density waves appear for $\lambda = 0.0, 0.1$. The small disturbances dissipate for $\lambda = 0.2$ as time goes on.

When $\lambda = 0.0$ in Fig. 5, it exhibits the space-time evolution of the headway for the coexisting phase after a sufficiently long time. The kink-antikink density waves appear as traffic jams. From the theoretic aspect, the traffic flow of $\lambda = 0.0$ in Fig. 5 with the given parameters is in the unstable flow region, and the kink-antikink density waves appear as traffic jam.

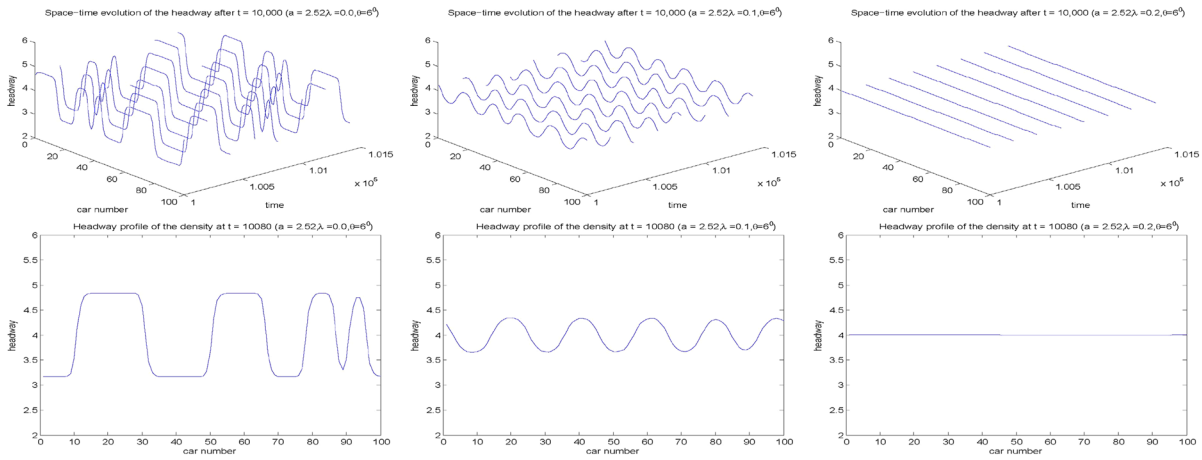

Fig. 7 Space–time evolution after $t = 10,000$ and corresponding headway at $t = 10,080$ of the density wave on a downhill slope 6°

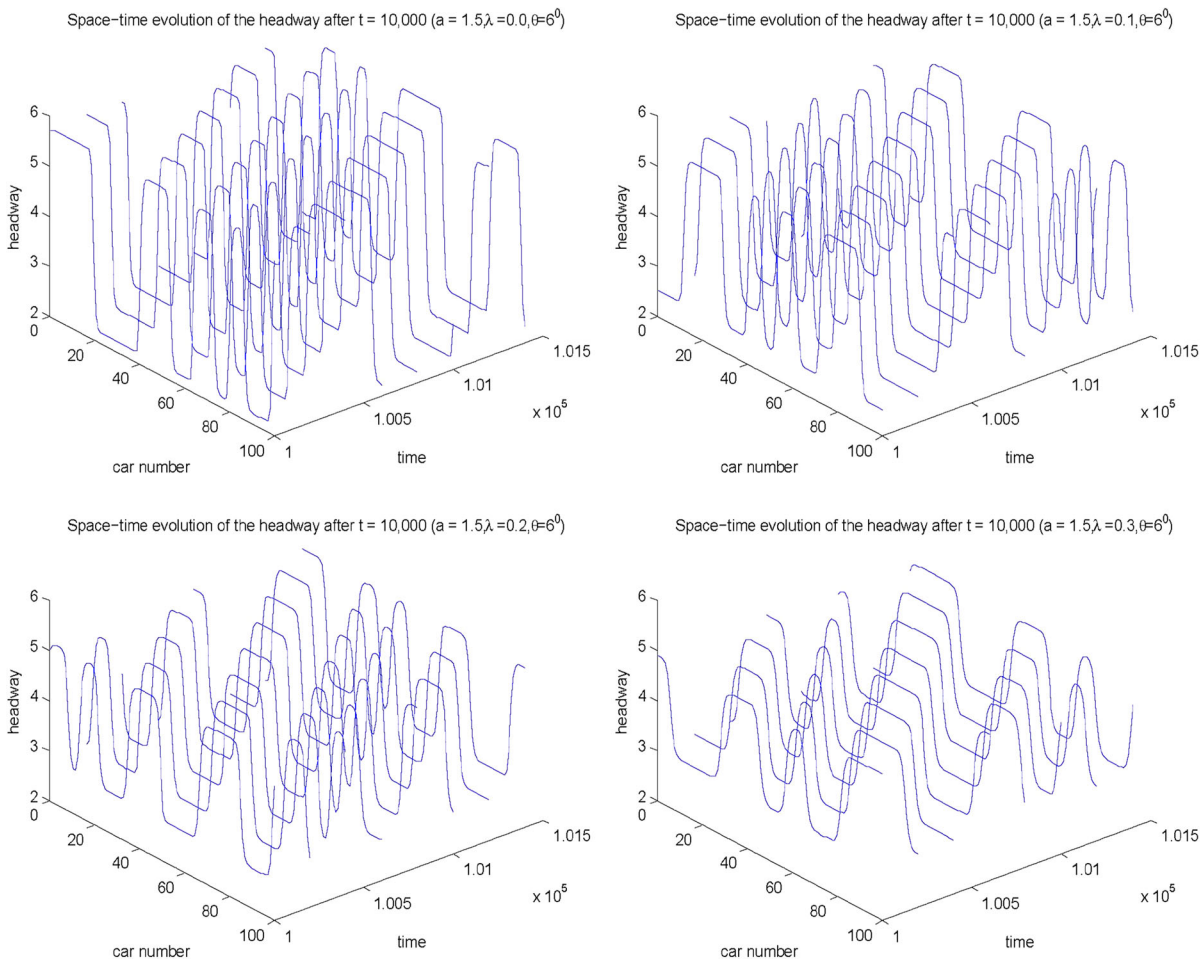

Fig. 8 Space–time evolution of the headway after $t = 10,000$ on a uphill slope 6°

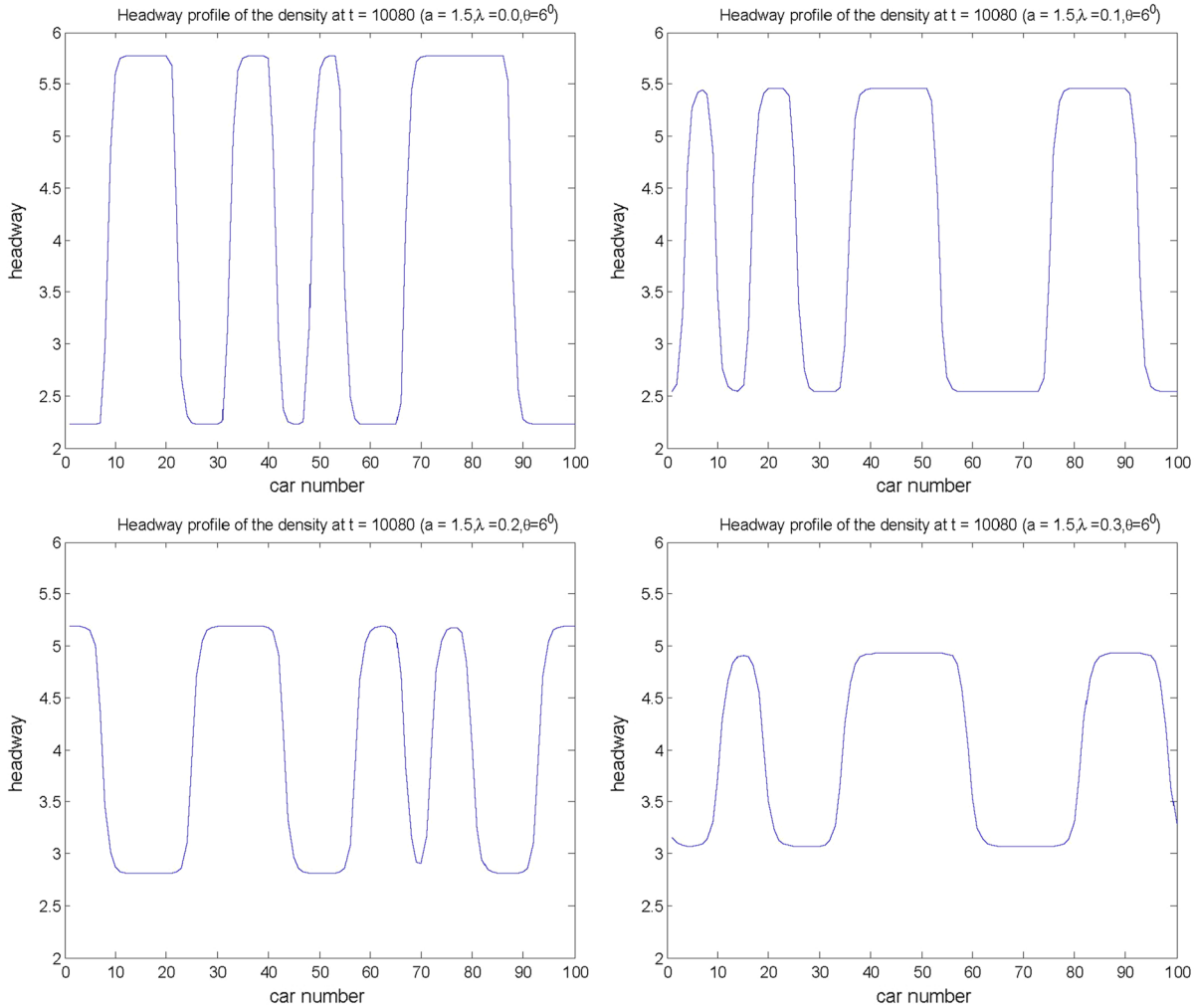

Fig. 9 Headway profile of the density wave at $t = 10,080$ correspond to Fig. 8 respectively

When $\lambda = 0.1$ in Fig. 5, it exhibits the space-time evolution of the headway after a sufficiently long time. The soliton density waves appear as traffic jams. From the theoretic aspect, the traffic flow of $\lambda = 0.1$ in Fig. 5 with the given parameters is near the neutral stability line and in the metastable flow region and the soliton density waves appear as traffic jam.

When $\lambda = 0.2$ in Fig. 5, it exhibits the space-time evolution of the headway for the freely moving phase after a sufficiently long time. For $\lambda = 0.2$, the density waves disappear, and traffic flow is uniform over the whole space.

Figure 6 shows the typical traffic patterns after a sufficiently long time $t = 10^4$ with different λ for $a = 2.4$ on uphill highway with slope $\theta = 6°$. Figure 6 exhibits the time evolution of the headway and correspond headway profile obtained at $t = 10,080$ for $\lambda = 0.0, 0.1, 0.2$. By using the linear stability condition (19), the traffic flow is linear unstable for $\lambda = 0.0, 0.1$. The traffic flow is stable for $\lambda = 0.2$. So the small disturbances will be amplified, and the density waves appear for $\lambda = 0.0, 0.1$. The small disturbances dissipate for $\lambda = 0.2$ as time goes on.

When $\lambda = 0.0$ in Fig. 6, it exhibits the space-time evolution of the headway for the coexisting phase after a sufficiently long time. The kink-antikink density waves appear as traffic jams. From the theoretic aspect, the traffic flow of $\lambda = 0.0$ in Fig. 6 with the given parameters is in the unstable flow region, and the kink-antikink density waves appear as traffic jam.

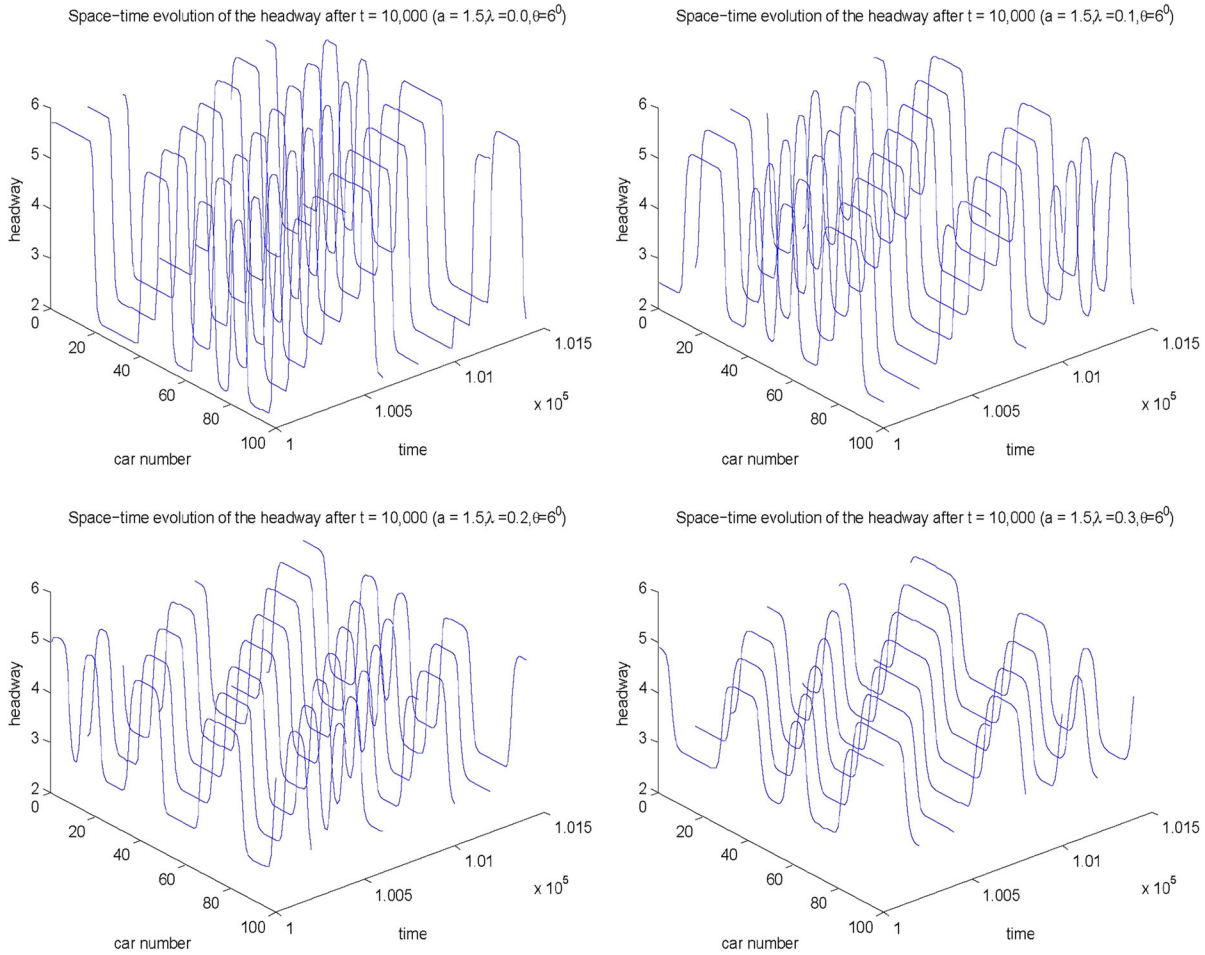

Fig. 10 Space–time evolution of the headway after $t = 10,000$ on a downhill slope 6°

When $\lambda = 0.1$ in Fig. 6, it exhibits the space-time evolution of the headway after a sufficiently long time. The soliton density waves appear as traffic jams. From the theoretic aspect, the traffic flow of $\lambda = 0.1$ in Fig. 6 with the given parameters is near the neutral stability line and in the metastable flow region, and the soliton density waves appear as traffic jam.

When $\lambda = 0.2$ in Fig. 6, it exhibits the space-time evolution of the headway for the freely moving phase after a sufficiently long time. For $\lambda = 0.2$, the density waves disappear, and traffic flow is uniform over the whole space.

Figure 7 shows the typical traffic patterns after a sufficiently long time $t = 10^4$ with different λ for $a = 2.52$ on downhill highway with slope $\theta = 6°$. Figure 7 exhibits the time evolution of the headway and corresponds headway profile obtained at $t = 10,080$ for $\lambda = 0.0, 0.1, 0.2$. By using the linear stability condition (19), the traffic flow is linear unstable for $\lambda = 0.0, 0.1$. The traffic flow is stable for $\lambda = 0.2$. So the small disturbances will be amplified, and the density waves appear for $\lambda = 0.0, 0.1$. The small disturbances dissipate for $\lambda = 0.2$ as time goes on. From Fig. 7, we can obtain the similar conclusions, that is, when $\lambda = 0.0$ in Fig. 7, the traffic flow is unstable, and the kink-antikink density waves appear as traffic jam; when $\lambda = 0.1$ in Fig. 7, the traffic flow is metastable, and the soliton density waves appear as traffic jam; for $\lambda = 0.2$, the density waves disappear, and traffic flow is uniform over the whole space.

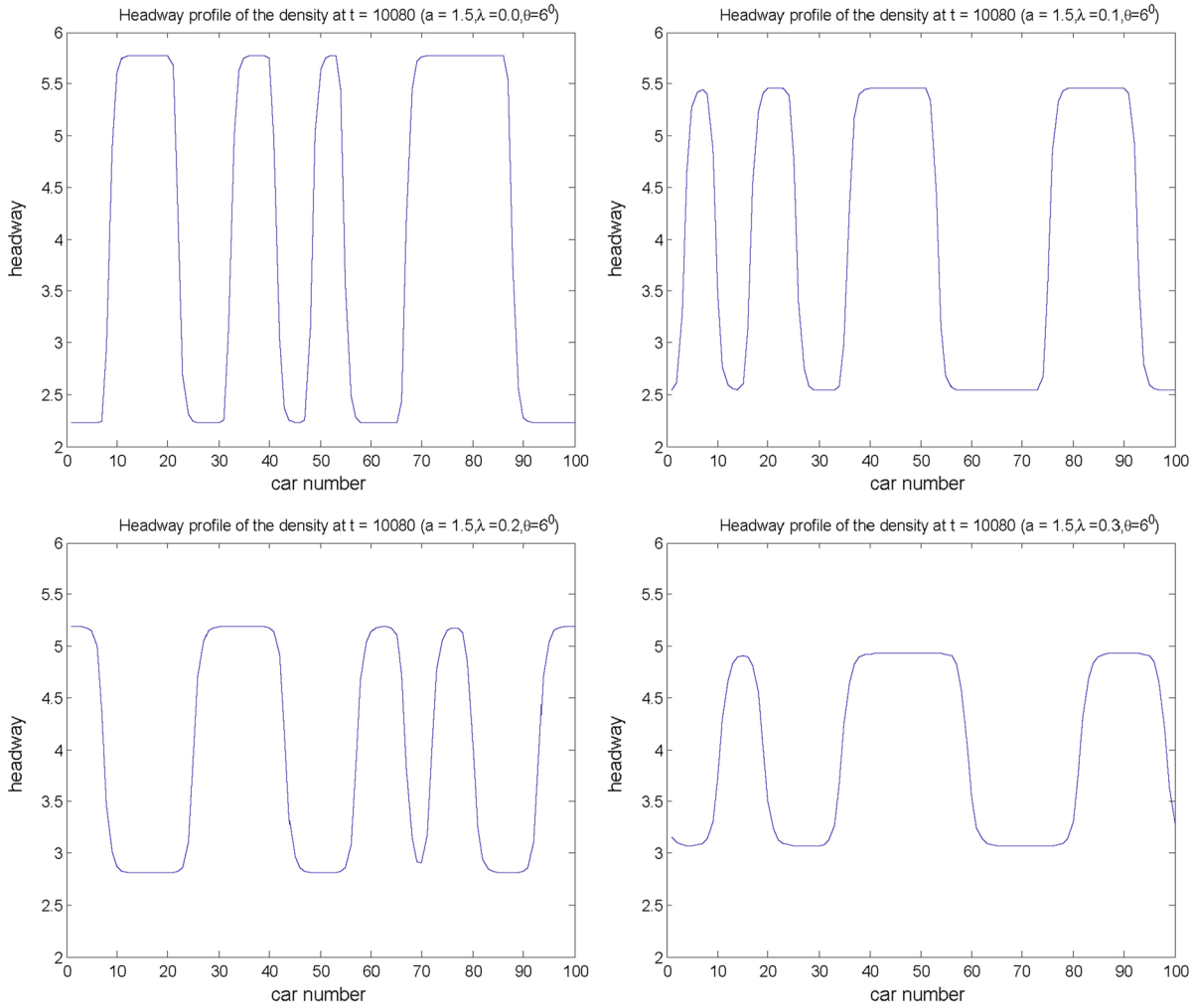

Fig. 11 Headway profile of the density wave at $t = 10,080$ correspond to Fig. 10, respectively

From Figs. 5, 6, and 7, we can see that by introducing the relative velocity which leads to the stabilization of the traffic flow.

Figure 8 shows the typical traffic patterns in the unstable region after a sufficiently long time $t = 10^4$ with different λ for $a = 1.5$ on uphill highway with slope $\theta = 6°$. Figure 8 exhibits the time evolution of the headway for $\lambda = 0.0, 0.1, 0, 2, 0.3$. As same as in Fig. 5, because the linear stability condition (19) is not satisfied, the traffic flow is linear unstable. But we find that the amplitude of the density wave decreases as λ increases. Figure 9 shows the headway profile obtained at $t = 10,080$ corresponding to Fig. 8, respectively. From Figs. 8 and 9, we find that in the unstable region the kink-antikink waves appear as traffic jams, and they propagate backwards.

Figure 10 shows the typical traffic patterns in the unstable region after a sufficiently long time $t = 10^4$ with different λ for $a = 1.5$ on downhill highway with slope $\theta = 6°$. Figure 10 exhibits the time evolution of the headway for $\lambda = 0.0, 0.1, 0, 2, 0.3$. The traffic flow is linear unstable, but we also find that the amplitude of the density wave decreases as λ increases. Figure 11 shows the headway profile obtained at $t = 10,080$ corresponding to Fig. 10, respectively. From Figs. 10 and 11, we see that the kink-antikink waves appear as traffic jams, and they propagate backwards in the unstable region.

5 Summary

We have investigated the effect of relative velocity upon traffic flow on a highway with uphill and downhill; we extend the model proposed by Komada et al. through taking the relative velocity into account. We obtain the stability condition of the extended FVDM by using linear stability theory. The stability condition shows that the slope and the relative velocity play an important role in influencing the stability of the traffic flow. The Burgers, KdV, and MKdV equations are obtained to describe the traffic behavior in the stable, metastable, and unstable flow region, respectively. The results show that the stability of traffic flow varies with different slopes, and the increase of λ leads to the stabilization of the traffic flow. When $\lambda = 0$, the results are consistent with those in previous work. The simulation results are consistent with the analytical ones.

The road visibility and mixed traffic may influence the driver's action in real traffic. In the Ref. [33,34], based on the optimal velocity model and FVDM, the authors considered the mixed traffic flow and visual information of the follower's driver and proposed corresponding models. Thus, the model proposed in the paper can be developed by taking these factors into account, since the methods applied in the paper may also work in that case. However, it will be more complicated and the focus of the paper in considering the effect of relative velocity upon the traffic flow on a gradient highway. But taking visual information and mixed traffic into account will make the car-following model more realistic, so the visual information and mixed traffic in the gradient highway need to be investigated in the future.

Acknowledgments The authors wish to thank the anonymous referees for their useful comments. This work was partially supported by the National Natural Science Foundation of China (Grant No. 61134004; 11071284), Zhejiang Province National Science Foundation (Grant No. LY12F02022; LY12A01009), Zhejiang Province Educational Research Project(Grant No. Y201328023).

References

1. Pipes, L.A.: An operational analysis of traffic dynamics. J. Appl. Phys. **24**, 274–281 (1953)
2. Bando, M., Hasebe, K., Nakayama, A., Shibata, A., Sugiyama, Y.: Dynamics model of traffic congestion and numerical simulation. Phys. Rev. E **51**(2), 1035–1042 (1995)
3. Helbing, D., Tilch, B.: Generalized force model of traffic dynamics. Phys. Rev. E **58**(1), 133–138 (1998)
4. Jiang, R., Wu, Q.S., Zhu, Z.J.: Full velocity difference model for a car-following theory. Phys. Rev. E **64**(1), 017101 (2001)
5. Jiang, R., Wu, Q.S., Zhu, Z.J.: A new continuum model for traffic flow and numerical tests. Transp. Res. B **36**(5), 405–419 (2002)
6. Xue, Y., Dong, L.Y., Yuan, Y.W., Dai, S.Q.: The effect of the relative velocity on traffic flow. Commun. Theor. Phys. **38**(2), 230–234 (2002)
7. Peng, G.H., Cai, X.H., Liu, C.Q., Cao, B.F., Tuo, M.X.: Optimal velocity difference model for a car-following theory. Phys. Lett. A **375**(45), 3973–3977 (2011)
8. Kerner, B.S., Konhauser, P.: Cluster effect in initially homogeneous traffic flow. Phys. Rev. E **48**(4), 2335–2338 (1993)
9. Kurtze, D.A., Hong, D.C.: Traffic jams, granular flow, and soliton selection. Phys. Rev. E **52**(1), 218–221 (1995)
10. Komatsu, T., Sasa, S.: Kink soliton characterizing traffic congestion. Phys. Rev. E **52**(5), 5574–5582 (1995)
11. Nagatani, T.: Stabilization and enhancement of traffic flow by the next-nearest-neighbor interaction. Phys. Rev. E **60**(6), 6395–6401 (1999)
12. Li, Y.F., Zhu, H., Cen, M., Li, Y.G., Li, R., Sun, D.H.: On the stability analysis of microscopic traffic car-following model: a case study. Nonlinear Dyn. **74**, 335–343 (2013)
13. Xue, Y.: Analysis of the stability and density waves for traffic flow. Chin. Phys. **11**(11), 1128–1134 (2002)
14. Ge, H.X., Dai, S.Q., Dong, L.Y., Xue, Y.: Stabilization effect of traffic flow in an extended car-following model based on an intelligent transportation system application. Phys. Rev. E **70**(6), 066134 (2004)
15. Li, Y.F., Sun, D.H., Liu, W.N., Zhang, M., Zhao, M., Liao, X.Y., Tang, L.: Modeling and simulation for microscopic traffic flow based on multiple headway, velocity and acceleration difference. Nonlinear Dyn. **66**, 15–28 (2011)
16. Ngoduy, D.: Effect of driver behaviours on the formation and dissipation of traffic flow instabilities. Nonlinear Dyn. **69**(3), 969–975 (2012)
17. Li, X.L., Song, T., Kuang, H., Dai, S.Q.: Phase transition on speed limit traffic with slope. Chin. Phys. B **17**(8), 3014–3020 (2008)
18. Komada, K., Masakura, S., Nagatani, T.: Effect of gravitational force upon traffic flow with gradients. Physica A **388**(14), 2880–2894 (2009)
19. Kerner, B.S., Klenov, S.L., Hiller, A.: Empirical test of a microscopic three-phase traffic theory. Nonlinear Dyn. **49**(4), 525–553 (2007)
20. Zhu, W.X., Yu, R.L.: Nonlinear analysis of traffic flow on a gradient highway. Physica A **391**(4), 954–965 (2012)
21. Cross, M.C., Hohenberg, P.C.: Pattern formation outside of equilibrium. Rev. Mod. Phys. **65**, 851–1112 (1993)
22. Ge, H.X., Cheng, R.J., Dai, S.Q.: KdV and kink-antikink solitons in car-following models. Physica A **357**, 466–476 (2005)
23. Tang, T.Q., Wang, Y.P., Yang, X.B., Wu, Y.H.: A new car-following model accounting for varying road condition. Nonlinear Dyn. **70**(2), 1397–1405 (2012)
24. Zheng, L.J., Tian, C., Sun, D.H., Liu, W.N.: A new car-following model with consideration of anticipation driving behavior. Nonlinear Dyn. **70**(2), 1205–1211 (2012)

25. Helbing, D.: Traffic and related self-driven many-particle systems. Rev. Mod. Phys. **73**(4), 1067–1141 (2001)
26. Lee, H.K., Lee, H.W., Kim, D.: Steady-state solutions of hydrodynamic traffic models. Phys. Rev. E **69**(1), 016118 (2004)
27. Jamison, S., McCartney, M.: A velocity matching car-following model on a closed ring in which overtaking is allowed. Nonlinear Dyn. **58**, 141–151 (2009)
28. Nagatani, T., Nakanishi, K.: Delay effect on phase transitions in traffic dynamics. Phys. Rev. E **57**(6), 6415–6421 (1998)
29. Bando, M., Hasebe, K., Nakanishi, K., Nakayama, A.: Analysis of optimal velocity model with explicit delay. Phys. Rev. E **58**(5), 5429–5435 (1998)
30. Muramatsu, M., Nagatani, T.: Soliton and kink jams in traffic flow with open boundaries. Phys. Rev. E **60**(1), 180–187 (1999)
31. Nagatani, T.: Density waves in traffic flow. Phys. Rev. E **61**(4), 3564–3570 (2000)
32. Yu, L., Li, T., Shi, Z.K.: Density waves in a traffic flow with reaction-time delay. Physica A **389**, 2607–2616 (2010)
33. Yang, D., Jin, P., Pu, Y., Ran, B.: Stability analysis of the mixed traffic flow of cars and trucks using heterogeneous optimal velocity car-following model. Physica A **395**, 371–383 (2014)
34. Sheng, J., Wang, D.H., Huang, Z.Y., Tao, P.F.: Visual angle model for car-following theory. Physica A **390**, 1931–1940 (2011)